5th Joint International Symposium on Deformation Monitoring (JISDM), 20-22 June 2022, Valencia, Spain
DOI: http://doi.org/10.4995/JISDM2022.2022.13813

Vibration monitoring of a bridge using 2D profile laser scanning: Lessons learned from the comparison of two spatio-temporal processing strategies

Nicholas Meyer, Lorenz Schmid, Andreas Wieser, Tomislav Medic

Institute of Geodesy and Photogrammetry, ETH Zürich, Stefano-Franscini-Platz 5, 8093 Zürich, Switzerland, (nicholas.meyer@geod.baug.ethz.ch; lorenz.schmid@geod.baug.ethz.ch; andreas.wieser@geod.baug.ethz.ch; tomislav.medic@geod.baug.ethz.ch)

Key words: *structural health monitoring; deformation monitoring; oscillations; LiDAR; point clouds*

ABSTRACT

Profile laser scanning allows sub-millimeter precise contact-free measurements with high spatial and temporal resolution. That makes it an appealing solution for structural health monitoring focusing on vibrations of engineering structures, such as the analysis of eigenmodes and eigenfrequencies of bridges. In this work, we use the profile scanning mode of a Zoller+Fröhlich Imager 5016 terrestrial laser scanner (TLS) to observe bridge dynamics, focusing on the free decay processes following trains passing the bridge and exciting the structure. We compare two vibration monitoring strategies and implement an open-source semi-automatic software that integrates both approaches. We successfully estimate a spatio-temporal vibration model (including dampening coefficient) despite the maximum vibration amplitude reaching only 0.3 mm during the free decay process. Both strategies allow the estimation of the first eigenfrequency with a precision better than 0.1 Hz. Within the paper, we highlight the advantages and tackle the identified challenges of these vibration monitoring strategies. We also report on a preliminary investigation of appropriate instrument positioning for estimating the parameters of a spatio-temporal vibration model.

I. INTRODUCTION

Scanners are progressively more used for structural health monitoring (SHM) of civil engineering structures (Mukupa *et al.*, 2017). Changes in geometry of 3D point clouds are used to monitor dams, bridges and tunnels under load or over time (Neuner *et al.*, 2016). Often, the analysis aims at low-frequency phenomena, *e.g.*, causing deformations on time scales from hours to years.

A special case of SHM with scanners introduced recently in Schill (2018) focuses on monitoring high-frequency phenomena, *e.g.*, geometry changes occurring with a frequency of 1 Hz or higher. In such applications, repeated 2D vertical profiles are typically collected instead of full 3D geometry to achieve coverage with sufficiently high frequency. The strategy was successfully used to characterize bridge deformations due to passing traffic, as well as for the vibration monitoring focusing on the free decay process after the bridge excitation (Schill and Eichhorn, 2019). It allowed for quantification of eigenfrequencies and related amplitudes nearly continuously over the whole bridge. The approach relies on a careful point cloud preprocessing, locally applying classical signal processing techniques (fast Fourier transform - FFT) and stacking this locally extracted information to get an overview of the behavior of the entire bridge.

Holst and Neuner (2021) proposed an additional processing step, estimating the optimal spatiotemporal vibration model within a least-squares (LS) adjustment. This offers several advantages, e.g., it increases sensitivity by improving the Nyquist frequency as compared to (half) the profile scan repetition rate. The authors validated this approach on a simulated dataset only, and its transfer to real-world applications requires tackling some challenges (see Section II B).

Within this work, we implemented both approaches and combined them in a single open-source software[1]. We tackled the mentioned challenges of the approach proposed in Holst and Neuner (2021), and successfully applied it to a real dataset: profile scans of a railway bridge in a free decay process following a train passing over. We conducted an eigenmode analysis and compared the results of both approaches against results obtained from multiple input multiple output synthetic aperture radar (MIMO-SAR), *i.e.*, an independent technology, confirming the plausibility of the estimated quantities. As a recommendation for the practitioners, we preliminarily analyzed the impact of the choice of the scanner position on the vibration monitoring results. Finally, we discuss relevant further development steps of the implemented software.

The article is organized as follows: Section II provides an overview of the mentioned vibration monitoring approaches (A – Schill and Eichhorn, 2019; B – Holst and Neuner, 2021) and presents our implemented workflow (C). Section III introduces the conducted experiment. The results and discussion are given in Section IV.

[1] Source-code available at *https://github.com/NixtonM/VM2dPLS*

II. METHODS

A. *Schill and Eichhorn (2019)*

The monitoring strategy proposed by Schill and Eichhorn (2019) primarily focuses on a careful point cloud pre-processing and provides a simplified vibration analysis in comparison to the approach by Holst and Neuner (2021) shown later in this section. The main goals of pre-processing are removing all scanned points not corresponding to the main structure of the bridge, removing outliers, and reducing the noise level, as the typical vibration amplitudes fall below the noise level of a single TLS measurement. The point cloud segmentation is realized using connected component clustering (Samet and Tamminen, 1988). De-noising is carried out using one of the three following strategies: spatial clustering and averaging per cluster within each 2D profile, approximating each scanned profile with a B-Spline function, or de-noising each profile using a discrete wavelet transform (Shensa, 1992).

The eigenmode analysis is then realized by applying the FFT on time series of de-noised displacements for individual positions along the bridge. The resulting amplitude spectra are displayed together to generate a spatio-temporal representation (see *e.g.*, Figure 1), where the eigenfrequencies and corresponding amplitudes can be quantified visually.

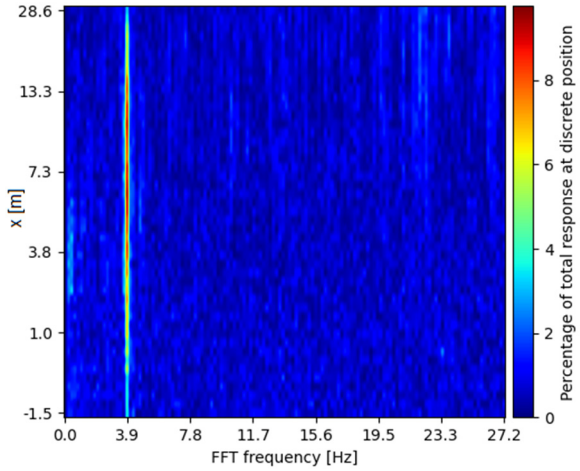

Figure 1. FFT amplitude spectra for discrete positions along the bridge (similar to results of Schill and Eichhorn, 2019).

B. *Holst and Neuner (2021)*

The strategy proposed by Holst and Neuner (2021) relies on processing profile scans (2D Cartesian coordinates x and y with per point time stamps t) within a LS adjustment with four different models differing by the prior knowledge or assumptions that are introduced within the functional and/or stochastic model. Here, we briefly present the two extreme cases which we implemented in the above software for the case of a single eigenfrequency. The first model is (Eq. 1):

$$y_{x_i}(t_i) = \bar{y}_{x_i} + A_{x_i} \cdot \sin\left(2\pi f_{x_i} t_i + \varphi_{x_i}\right) \qquad (1)$$

where t_i is the measurement time stamp, $y_{x_i}(t_i)$ is the observed vertical coordinate of point i, and this point is defined by its horizontal coordinate x_i along the bridge (given value). The searched eigenmode parameters are: $\bar{y}_{x_i}$- vertical position of the bridge at steady state (*i.e.*, mean position), A_{x_i} – vibration amplitude, f_{x_i} – frequency and φ_{x_i} – phase-shift. Using all observations and a Gauss-Markov model (GMM) the authors estimate an independent set of 4 parameters for each x_i, describing the vibration as a function of time for the respective location. Here, the encoded prior knowledge is only: A) each part of the bridge oscillates according to a single sine function around its steady-state position; and B) the deformation occurs in the vertical direction. Although this may not be realistic, this model imposes no spatial correlation of the vibration patterns and allows for (arbitrarily) different amplitudes along the bridge.

The second realization introduces additional prior assumptions: C) all positions along the bridge x_i have a common oscillation frequency and phase shift; D) there is a common amplitude, which is a sine function of space (x_i) according to a single beam vibration model; E) the steady-state of the bridge (bridge shape and position in space) can be approximated by a function. This realization is represented by (Eq. 2):

$$y(x,t) = d \cdot x + b + A \cdot \sin\left(2\pi f_x x + \varphi_x\right) \cdot \sin\left(2\pi f_t t + \varphi_t\right) \qquad (2)$$

where d and b are parameters used for linear approximation of the bridge shape and position at steady state; A is a vibration amplitude, f_x and φ_x are frequency and phase-shift in space (x_i), while f_t and φ_t are frequency and phase-shift in time (t_i); y are observations, and x and t are given.

This second realization provides a spatio-temporal vibration model. However, it comes with the disadvantage of introducing additional nonlinearities in the functional model (additional spatial sine function). As all parameters are correlated, the solution becomes increasingly sensitive to the quality of initial parameter values. Even a small deviation (several percent off from the true value) can cause incorrect adjustment convergence.

A detailed analysis of this sensitivity is out of the scope of our work. However, it poses a significant challenge for transferring the approach to real measurement data, which was tackled within the implemented workflow (see C). Additionally, we observed that the correct convergence of the second realization depends on the instrument position with respect to the measurement subject, which will be further elaborated in Section IV.

C. *Implemented workflow*

The implemented workflow is summarized in Figure 2 and consists of a *Data Pre-Processing* step and three consecutive LS parameter estimation steps (*temporal*, *spatial*, and *combined*).

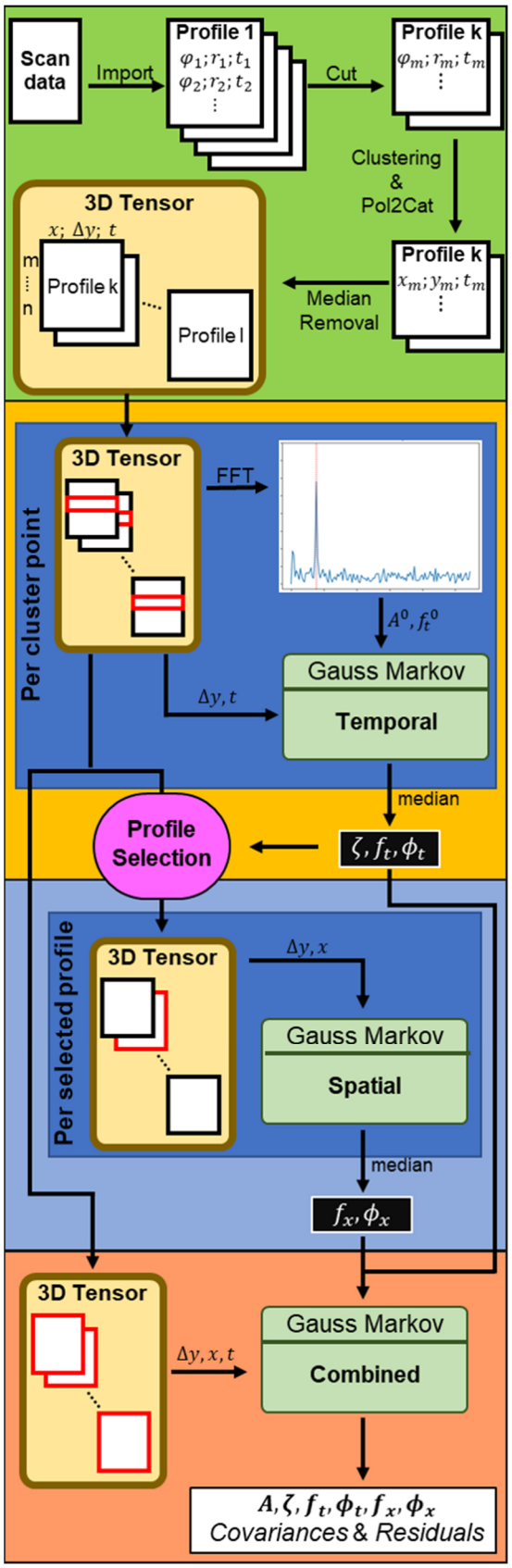

Figure 2. Flowchart of the implemented workflow.

The output of each adjustment step either narrows down the number of observation equations or determines the initial parameter values for the subsequent adjustment. The final adjustment provides the parameters for a combined spatio-temporal vibration model adapted from Holst and Neuner (2021). Due to practical considerations, we expand Equation 2 herein by a term describing the damping (with dampening coefficient ζ), and the linear approximation of the bridge shape at rest is replaced by median value reduction per location in the *data pre-processing* step. The resulting functional model for the displacements in the vertical is represented by (Eq. 3):

$$\Delta y(x,t) = Ae^{-\zeta \cdot t} \cdot \sin(2\pi f_x x + \varphi_x) \cdot \sin(2\pi f_t t + \varphi_t) \qquad (3)$$

Within the *Data Pre-Processing* step, we first retain only the measurements inside of the time window and field-of-view of interest (through the user interface). This is followed by spatial clustering wherein each profile is segmented by a common set of evenly spaced elevation angle boundaries, resulting in point clusters containing roughly the same number of points. Depending on point density due to the measurement range and angle of incidence, this approach results in varying spatial extents of the clusters (Figure 3). If the scanner output is in terms of polar coordinates (φ, r), we convert them to Cartesian (x, y). Furthermore, we calculate the median point per cluster, as one of the possible realizations of spatial low-pass filtering proposed by Schill and Eichhorn (2019). These median points are used in all further processing steps as: A) they provide a better signal-to-noise ratio (SNR) than raw observations; B) they remove the need to handle the varying number of points per profile (e.g., due to momentary occlusions); C) they assure more realistic parameter uncertainty estimates than when using raw observations, as the correlations between the observations are unknown and, hence, disregarded.

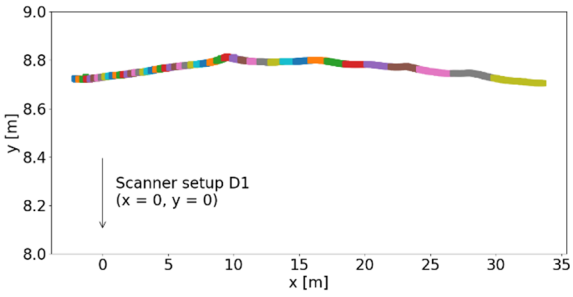

Figure 3. Implemented profile-wise spatial clustering (the example from the experiment in Section III).

In contrast to the simulations from Holst and Neuner (2021), we cannot model the shape of the bridge at the steady-state to the accuracy necessary with a simple function (Eq. 2). We therefore discretely approximate the shape of the bridge by calculating the median y values of each point over time. These values are subtracted from the y values of the points, thereby

transforming the height value of each point into a measure of displacement Δy from the steady-state in the vertical direction (Eq. 3).

In the *temporal* adjustment step, we simplify our functional model by removing the terms of Equation 3 that are dependent on the horizontal position x. To compensate for this simplification the adjustment is carried out for each point in space individually (Eq. 4):

$$\Delta y_x(t) = A_x \cdot e^{-\zeta \cdot t} \cdot \sin(2\pi f_t t + \varphi_t) \quad (4)$$

While the resulting sets of parameters differ in amplitude, the values for ζ, f_t and ϕ_t are ideally the same for all points in space. The starting values for f_t and A are acquired through the FFT on the time series of each cluster mean point, while ζ and ϕ_t are set to 0. The results of this step are gathered by calculating the parameters' medians after correcting the values for their cyclic nature. The amplitude spectra resulting from the abovementioned FFT are used to generate a spatio-temporal representation of observed vibrations (*e.g.*, Figure 1), which corresponds to the results of Schill and Eichhorn (2019).

In the spatial adjustment step, we again simplify Equation 3 by removing the terms dependent on time and calculating the adjustment on individual profiles (Eq. 5):

$$\Delta y_t(x) = A_t \cdot \sin(2\pi f_x \mathrm{x} + \varphi_x) \quad (5)$$

Since most profiles have a very poor SNR when describing their displacement in the context of an idealized sinusoidal, we first reduce the number of profiles to those with maximal displacement from the steady-state. This is done by determining the median time for each profile and using these values in conjunction with the previously acquired temporal parameters to calculate a maximum amplitude factor. We then select only those profiles for which the maximum amplitude factor falls within the top 10%. In contrast to the previous adjustment step, the determination of the starting values cannot be achieved with FFT as our observations only capture the section of the bridge between two of its piers, which based on our assumed model has the extent of half of the spatial wavelength of the first eigenfrequency. We, therefore, use the horizontal distance between the two piers to compute the starting value of f_x, where f_x^0 is the inverse of two times the length of the observed structure. The amplitude A is set to the maximum value within each profile and the phase shift ϕ_x is set to 0. Again, the results for f_x and ϕ_x are gathered by determining the median values.

In the *combined* adjustment step we finally estimate the parameters of Equation 3, their uncertainty estimates and observation residuals using all observations (covariance matrix = identity matrix). The starting values are set according to the results of the previous steps.

III. Experiment

The implemented software was tested on a case study of vibration monitoring of a segment of the Hardbrücke railway bridge in Zürich, Switzerland. The bridge is realized as a simple reinforced concrete beam bridge supported by regularly spaced pillars (Figure 4). The bridge serves as a dedicated cargo train bridge.

We measured on two days (D1: October 18, 2021, and D2: January 5, 2022) using the profile scanning mode of a Zoller+Fröhlich Imager 5016. The scanner was placed at different positions under the investigated bridge segment on the two days: at the end of the segment on D1, and in the middle of the span on D2, see Figure 4. We acquired 2D profiles along the main bridge direction by manually aligning the scanning direction. The scanner was placed centrally considering the bridge width.

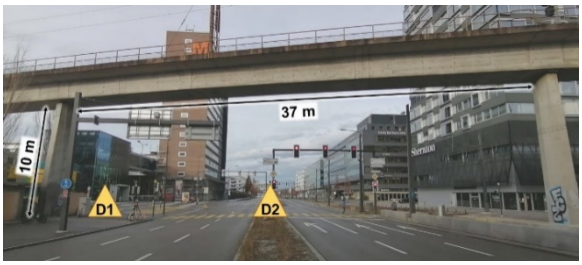

Figure 4. Investigated bridge segment and scanner positions at both measurement days (D1 and D2).

On the second day, a MIMO-SAR instrument was used in addition to the scanner to serve as an independent validation. The readers are referred to Baumann-Ouyang *et al.* (2022) for more information about that sensor and the measurement process.

The outcome of measurements at each day are time series lasting several minutes containing the following events: 1 – bridge at steady state, 2 – train passing over the bridge causing deformations, 3 – free decay process after unloading of the bridge, 4 – bridge at steady state again (Figure 5). The data analysis focused on analyzing the free decay process (3 in Figure 5), during which the structure is left vibrating in an excited state with its natural frequency for several seconds. As the trains passing the bridge were different on each day (*e.g.*, different length, weight, and speed), the time series of the free decay process were expected to be slightly different. This primarily refers to the maximum observed vibration amplitude, while the eigenfrequency and other structure-related parameters are expected to be the same.

During these several minutes, the measurement conditions (measurement configuration, atmospheric conditions, etc.) remained stable. Hence, no systematic influences are expected to impact the results of the analysis. To assure high measurement stability and avoid eventual vibrations of the instrument itself (*e.g.*, due to wind gusts), the instrument was placed on a heavy-duty scanning tripod at its lowest possible setup height. The measurements were conducted with the

following scanner settings: maximal mirror rotation speed of 52 Hz, lowest quality (minimal spatial point averaging), and maximal spatial resolution within each profile (0.8mm@10m). The expected range measurement noise of a single point was approximately 0.4 mm according to the manufacturer's specifications.

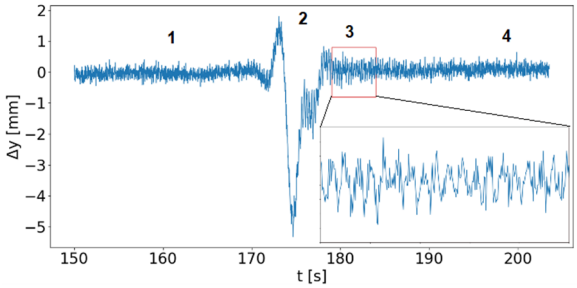

Figure 5. Time series of vertical displacements for D1 (numbers denoting different events).

IV. Results and Discussion

This section contains: A) the results of the implemented workflow and discussion of the results in the context of two presented vibration monitoring strategies (Section II A and B); B) analysis of the impact of measurement configuration; and C) discussion about the further development of the implemented workflow.

A. *Results of the implemented workflow*

The intermediate results of the implemented workflow are amplitude spectra resolved along the bridge. Figure 1 visualizes the results for D1, while the results for D2 are negligibly different (see Table 1). The amplitudes are expressed as relative values over the whole spectrum (a percentage of the total response). Nearly over the whole bridge length, there is a clear single dominant vibration frequency at 3.834 Hz. The maximum amplitudes are detected approximately at the middle of the examined bridge segment, and they diminish towards the supporting pillars carrying it, which is expected for the first eigenfrequency of a simple beam model (a reasonable approximation for this bridge).

Table 1. Estimated vibration model parameters (D1 - the result of combined LS adjustment together with the uncertainty estimates, D2 – median results of temporal LS adjustments, and eigenfrequency estimated using MIMO SAR)

	D1		D2	MIMO SAR
	estim.	Std	estim.	estim.
A [mm]	0.280	0.006	0.139	
ζ [1/s]	0.142	0.008	0.142	
f_t [1/s]	3.789	0.001	3.803	3.850
ϕ_t [rad]	2.789	0.019	0.284	
f_x [1/m]	0.0130	0.0002		
ϕ_x [rad]	0.227	0.013		

These results equal the results of the approach presented in Schill and Eichhorn (2019), with one clear distinction. In the latter study, the authors succeeded to distinguish the first two eigenfrequencies using a similar instrument (dedicated 2D profiling scanner, Z+F Profiler 9012) and a similar experimental setup. If this is due to the differences in the experimental design, the used instrument (standard TLS vs. profiling scanner) or the object under investigation, should be further examined. However, this is out of the scope of this work. Here, we only confirm that preprocessed profile scans of a standard "3D" terrestrial laser scanner can be used to quantify eigenfrequency and vibration magnitude already by calculating spatially resolved amplitude spectra. The plausibility of these scanning-based results was confirmed with a MIMO SAR, where we analyzed a single amplitude spectrum for a narrow region in the middle of the investigated bridge segment (see Table 1).

The final output of the implemented workflow is an estimated vibration model describing the bridge vibration in space and time. The parameters and their uncertainty values are presented in Table 1. These results correspond to the results of the approach presented in Holst and Neuner (2021), which is herein successfully applied to a real dataset for the first time to the best of our knowledge. The final *combined* LS adjustment (Section III C) converged to unrealistic parameter values for D2. We attribute this to the unfavorable measurement configuration (see Section IV B). We thus report the median of the temporal LS adjustment results for D2 in Table 1.

There are several advantages of this extended analysis beyond the amplitude spectra presented in Figure 1. First, there is the possibility of estimating the dampening coefficient, which is relevant for SHM (Cao *et al.*, 2017). Our results indicate that the dampening coefficient can be well estimated using profile scanning, which is confirmed by: 1 – good agreement between D1 and D2, and 2 – by analyzing the adjustment residuals (Figure 6). The residuals show no apparent systematic behavior which would indicate an inadequate functional model that would be present in the data if the dampening coefficient was lacking or was incorrectly estimated. The only visible systematic behavior is due to the expected increase of the measurement noise with the increased distance and angle-of-incidence from the scanner (more in Section IV B).

The secon advantage of the extended analysis are the parameter uncertainty estimates. Having them is indispensable for rigorous statistical testing of the hypothesis "*the structure retained the expected material properties since the last measurements*", which signalizes good structural health. In the case of the simplified data analysis from Schill and Eichhorn (2019), similar estimates are lacking.

Moreover, having a full spatio-temporal vibration model is indispensable for simulations and comparison with the designed structure behavior. However, the main potential of the SHM with the high spatial

resolution offered by profile scanning is a possibility to analyze if the structure is locally behaving differently than expected.

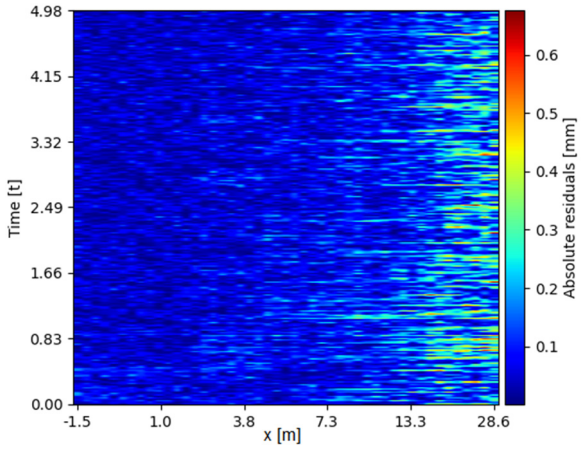

Figure 6. 2D Plot of the "*combined*" adjustment residuals.

Namely, obtaining the spatio-temporal model allows for systematically analyzing the adjustment residuals in the search for systematic patterns that would highlight unexpected building behavior. Additionally, by functionally modeling the detectable eigenmodes, they can be optimally removed from the measurement time series. Hence, analyzing the adjustment residuals which are free of their influence can increase the sensitivity of these local inspections. With the classical signal processing techniques, it is possible to filter out certain frequency bands corresponding to the frequencies with high oscillation amplitudes (approx. eigenfrequencies). However, due to possible spectral leakage (Harris, 1978), this could cause a loss of potentially relevant data.

To conclude, there are multiple benefits of the extended effort of obtaining the spatio-temporal deformation model proposed in Holst and Neuner (2021) from the data processing perspective. It remains to be analyzed in collaboration with structural engineers how this model needs to be adapted to properly reflect the physically determined deformations of the structure. In case of insufficient data quality for convergence of the full algorithm or if the model by Holst and Neuner (2021) is not justified from a structural point of view, using the simplified analysis from Schill and Eichhorn (2019) is preferable for estimating spatially resolved eigenfrequencies and vibration amplitudes.

B. *Influence of measurement configuration*

Our experiments revealed that the selection of the scanner position has a notable impact on the success of estimating the spatio-temporal vibration model. Namely, we were able to obtain the "*combined*" spatio-temporal model only for D1 (Table 1), while for D2 the workflow failed after the *temporal* LS adjustment step (Section II C). The reason can be found in the SNR which is influenced by the spatial vibration pattern and measurement configuration. The noise increases with distance and incidence angle (Soudarissanane *et al.*, 2011), while for the frequency of the first eigenmode, the amplitude diminishes from the bridge middle towards the supporting pillars (Figure 1).

Figure 7 presents the time series of a free decay process (Figure 5, event 3) for two locations along the bridge, the end (top) and the middle (bottom) of the investigated segment. The data are presented for D1 (blue) and D2 (orange) with different measurement configurations (Figure 4). Positioning the instrument directly in the middle of the investigated segment (D2) achieves the overall highest SNR directly above the scanner (Figure 7, bottom orange). However, at the same time, it achieves the overall worst SNR at the end of the segment, making the periodic signal due to natural frequency unobservable (Figure 7, top orange). This has a negative impact on estimating the complete spatio-temporal model, because it does not contain sufficient information for resolving the spatially related vibration parameters (f_x, φ_x in Eq. 3).

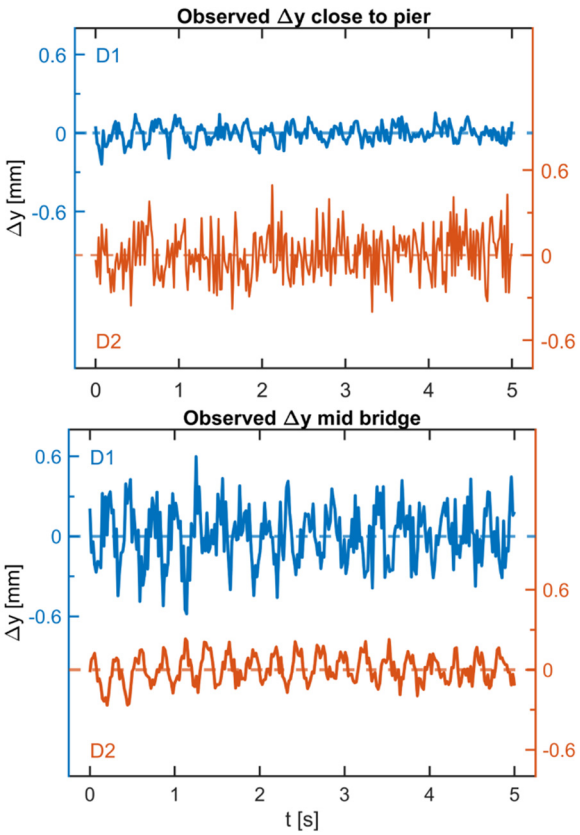

Figure 7. Time series of vertical displacements during a free decay process for D1 (blue) and D2 (orange) at the end (top) and the middle (bottom) of the bridge segment (y-axis presenting Δy in mm).

On the contrary, positioning the scanner at one end of the observed bridge segment (D1) assures overall lower, but more constant SNR along half of the segment. This leads to successfully estimating spatio-temporal vibration model (Table 1). Hence, this simplistic analysis indicates that for obtaining the

spatio-temporal vibration model, it is better to assure adequate SNR at the locations where the vibration amplitudes are expected to be small (close to the supporting bridge pillars). In our case, this is achieved by placing an instrument at one end of the observed bridge segment, which relies on the presumption of symmetrical bridge behavior (given by the functional model in Equation 3. Ideally, two instruments should be synchronized and used simultaneously at both ends of the investigated segment, which would lead to adequate SNR over the whole spawn.

C. *Further development of implemented workflow*

The workflow described in Section II C, is a prototypical implementation with some practical simplifications. Hence, there are multiple possibilities for its further development.

One direction is further automation of the approach, to reduce the need for human intervention. For example, eigenmode analysis could be further automated by detecting the free decay process within the measurement time series using a continuous wavelet transform. Moreover, the current implementation requires manually selecting the functional model. The former could be resolved by automatically testing a range of plausible functional models and identifying the most suitable one, *e.g.*, by using one of the established approaches to model selection. Also, the current implementation hard-coded the knowledge about the deformation direction (Eq. 3, deformations solely occur along the y-axis). A more general approach (*e.g.*, extending to vertical structures) should incorporate a functional model, which is defined in a more general sense.

The second direction of development is refining the point cloud pre-processing steps, *e.g.*, by further optimizing de-noising, implementing outlier removal, and optimizing spatial cluster sizes (as a trade-off of improved SNR and reduced sampling frequency). Moreover, some additional processing steps such as inducing stochastic resonance (Gammaitoni *et al.*, 1998) could further improve the sensitivity of the approach.

The third direction is refining the parameter estimation, *e.g.*, by incorporating a stochastic model of the scanner's genuine polar coordinates. Here, it would be advisable to refine a stochastic model by accounting for measurement degradation with a higher incidence angle (*e.g.*, observable in Figure 6), and by introducing variance component estimation (VCE). Also, the functional model could be expanded to model the shape of the object's surface (*e.g.*, using B-Splines or polynomials). Finally, the discussed high sensitivity of the LS adjustment towards the quality of the initial parameter values could be mitigated by implementing global heuristic optimizers with a bounded domain of possible parameter values, either as a substitute or as an addition to the currently implemented LS adjustment.

The last direction for development would be expanding the SHM analysis. One option is expanding it beyond analyzing the free-decay process, *e.g.*, by automatically detecting and functionally modeling the lower-frequency deformations (*e.g.*, caused by train crossing over the bridge), which would resemble classical load tests. Another option is developing already mentioned automatic analysis of the adjustment residuals to detect eventual local discrepancies relative to the expected global structure's behavior.

V. Conclusion

In this paper, we report about the implementation of a workflow for vibration monitoring using 2D profile laser scanning, which combines the strategies proposed in Schill and Eichhorn (2019), and Holst and Neuner (2021) and about preliminary results obtained by applying the workflow to data from. We used the prototypical implementation of the open-source software for the eigenmode analysis of a railway bridge based on 2D profiles acquired with a standard terrestrial laser scanner (TLS). We estimated a spatiotemporal vibration model including dampening coefficient from observations obtained shortly after a cargo train had passed over the bridge and had induced oscillations at the bridge's natural frequency of about 3.8 Hz with an amplitude as low as 0.3 mm.

The interpretation of the results obtained using two different measurement configurations indicated that it is better to place the instrument close to the bridge piers, and not in the middle of the inspected bridge segment (the most intuitive position) for estimating the parameters of a spatio-temporal vibration model. Starting from the results obtained herein, we discussed several recommended options to further develop the implemented workflow, ideally in collaboration with structural engineers to support the selection of spatio-temporal models representing the respective structure appropriately.

VI. Acknowledgements

Andreas Baumann provided and processed the MIMO-SAR data.

References

Baumann-Ouyang, A., Butt, J. and Wieser, A. (2022) Bridge deformations during train passage: monitoring multiple profiles using concurrently operating MIMO-SAR sensors. In: 5th Joint international *Symposium on Deformation Monitoring (JISDM)*. Valencia, Spain.

Cao, M.S., Sha, G.G., Gao, Y.F. and Ostachowicz, W. (2017) Structural damage identification using damping: a compendium of uses and features. *Smart Materials and structures*, 26(4), p. 43001.

Gammaitoni, L., Hänggi, P., Jung, P. and Marchesoni, F. (1998) Stochastic resonance. *Reviews of modern physics*, 70(1), p. 223.

Harris, F. J. (1978) On the use of windows for harmonic analysis with the discrete Fourier transform. *Proceedings of the IEEE*, 66(1), pp. 51–83.

Holst, C. and Neuner, H. (2021) Spatio-Temporal Models for Vibration Monitoring of Elongated Structures Using Profile Laser Scans. *Remote Sensing*, 13(7), p. 1369.

Mukupa, W., Roberts, G.W., Hancock, C.M. and Al-Manasir, K. (2017) A review of the use of terrestrial laser scanning application for change detection and deformation monitoring of structures. *Survey Review*, 49(353), pp. 99–116.

Neuner, H., Holst, C. and Kuhlmann, H. (2016) Overview on Current Modelling Strategies of Point Clouds for Deformation Analysis. *Allgemeine Vermessungs-Nachrichten (AVN)*, 123(11–12), pp. 328–339.

Samet, H. and Tamminen, M. (1988) Efficient component labeling of images of arbitrary dimension represented by linear bintrees. *IEEE transactions on pattern analysis and machine intelligence*, 10(4), pp. 579–586.

Schill, F. (2018) *Überwachung von Tragwerken mit Profilscannern*. TU Darmstadt.

Schill, F. and Eichhorn, A. (2019) Deformation Monitoring of Railway Bridges with a Profile Laser Scanner. *ZfV-Zeitschrift für Geodäsie, Geoinformation und Landmanagement*, 2, pp. 109–118. doi: 10.12902/zfv-0248-2018.

Shensa, M. J. (1992) The discrete wavelet transform: wedding the a trous and Mallat algorithms. *IEEE Transactions on signal processing*, 40(10), pp. 2464–2482.

Soudarissanane, S., Lindenbergh, R., Menenti, M. and Teunissen, P. (2011) Scanning geometry: Influencing factor on the quality of terrestrial laser scanning points. *ISPRS Journal of Photogrammetry and Remote Sensing*, 66(4), pp. 389–399.